# Amplitude calibration guideline of TMRT and NSRT

Yuzhu Cui,<sup>1,2</sup> Kazuhiro Hada<sup>1,2</sup> on behalf of EAVN Science Working Group

<sup>1</sup> Mizusawa VLBI Observatory, NAOJ

<sup>2</sup> Department of Astronomical Science, SOKENDAI

October 2020

#### Abstract

This is a memo to provide some guidelines to calibrate EAVN data, especially for TMRT and NSRT. EAVN data including other stations can also refer to this process.

### 1 Observations

Table 1 and 2 summarizes the basic information of the 9 stations which form a core array of EAVN. The parameters listed here are from the EAVN status report. <sup>1</sup> Below we describe some more details about TMRT and NSRT. For details of KaVA stations, see Niinuma et al. (2014) [1] and Hada et al. (2017) [2].

Here we selected two representative epochs from the EAVN 2017 campaign as summarized in table 1. These observations were conducted on March 18th (observing code: a17077a; hereafter, a17077a) and March 27th (observing code: a17086a; hereafter, a17086a) at 22 and 43 GHz, respectively. Yonsei (KYS) did not join a17077a due to an issue at the site. TMRT participated in both epochs along with KaVA, while NSRT was only available at 22 GHz. The overall weather condition was good at each site except TMRT in a17077a and KUS in a17086a. For TMRT, antenna pointing calibration was made only at the beginning of each session. We observed M 87 as a primary target of the EAVN campaign while the other sources (3C 273, 1219+044, M 84) were observed as calibrators. In detail, a17077a lasted for 7 hours where scans of  $3C\ 273\ (6\ \text{min}) - 1219 + 044\ (4\text{min}) - M\ 87\ (47\ \text{min}) - M\ 84\ (4\ \text{min}) -$ RT Vir (4 min) were repeated for 6 cycles. a17086a were performed for 5 hours where scans of 3C 273 (6 min) - 1219+044 (2 min) - M87 (54 min) - M84 (2 min) - RT Vir (4 min) were repeated for 4 cycles. RT Vir (H<sub>2</sub>O/SiO masers) was inserted for a system/frequency check of the experiments. The recording rate was 1 Gbps (2-bit sampling) where a total bandwidth of 256 MHz was divided into eight 32-MHz intermediate frequency (IF) bands. Only left-hand circular polarization was received. All the data were correlated at the Daejeon hardware correlator installed in Korea Astronomy and Space Science Institute (KASI).

Figure 1 shows the opacity-corrected system temperature  $(T_{\text{sys}}^{\star})$  for four representative stations. We note that the opacity correction of TMRT was done manually which will be

<sup>&</sup>lt;sup>1</sup>https://radio.kasi.re.kr/eavn/files/Status\_Report\_EAVN\_2020A\_20191031.pdf

Location	Name	Array	$D^a$	$\operatorname{Lat}^{b}$	Lon.c	$Alt.^d$	$\eta^e$	(%)	HPB	$\overline{\mathrm{W}^f}$
			(m)	$(\circ)$	$(^{\circ})$	(m)	K	Q	K	Q
Tianma	TMRT	CVN	65	31.092	121.136	49.2	50	45	44	22
Nanshan	NSRT	CVN	26	43.471	87.178	2029	60	-	115	-
Mizusawa	MIZ	VERA	20	39.134	141.133	116	47	51	141	71
Iriki	IRK	VERA	20	31.748	130.440	574	47	44	149	78
Ogasawara	OGA	VERA	20	27.092	142.217	273	50	45	143	78
Ishigakijima	ISG	VERA	20	24.412	124.171	65	49	48	144	79
Tamna	KTN	KVN	21	33.289	126.460	452	60	63	126	63
Ulsan	KUS	KVN	21	35.546	129.250	170	63	61	124	63
Yonsei	KYS	KVN	21	37.565	126.941	139	55	63	127	63

Table 1: General information of the nine stations from EAVN array used in this paper. <sup>a</sup> Diameter of each dish. <sup>b</sup> Latitude. <sup>c</sup> Longitude. <sup>d</sup> Altitude. <sup>e</sup> aperture efficiency. <sup>f</sup> HPBW is Half Power Beam Width in arcsecond.

elaborated in section 2.1. Unfortunately, NSRT failed to obtain the system temperature information due to the malfunction of the data acquisition system. Nevertheless, the observing condition at NSRT was overall good and its amplitude was properly calibrated by taking advantage of the scans of the point source 1219+044. Another main issue was that the active surface controller of TMRT did not properly work in a17086a according to the observation feedback from the site. We will discuss the possible impact of this effect in section 3.

### 2 Data reduction processes

The EAVN data were calibrated in the standard manner of VLBI data reduction procedures. We used the National Radio Astronomy Observatory (NRAO) Astronomical Image Processing System (AIPS; [3]) software package for the initial calibration of visibility amplitude, bandpass and phase. Subsequent imaging/CLEAN and self-calibration were performed with the DIFMAP software [4]. More details are described in the following subsections.

Array	$N_{ m Ant}^a$	$N_{ m bl}^b$	$B^c \text{ (km)}$		$\theta^d \text{ (mas)}$		$\sigma_I^e (\mu Jy)$	
			$\min$	max	K	Q	K	Q
KaVA (1)	7	21	305	2270	1.24	0.63	155	268
KaVA+TMRT (2)	8	28	305	2270	1.24	0.63	95	165
KaVA+TMRT+NSRT (3)	9	36	305	5078	0.55	_	75	_

Table 2: <sup>a</sup> Number of antennas. <sup>b</sup> Number of baselines. <sup>c</sup> Baseline length. <sup>d</sup> Angular resolution. <sup>e</sup> Image sensitivity  $\sigma_I$  is the typical value adopted in the EAVN status report under the assumption of an integration time t=4 hours and a total bandwidth  $B=256\,\mathrm{MHz}$ 

#### 2.1 Amplitude calibration

Amplitude calibration was performed to recover the correct source flux density from the observed raw data. Following the initial inspections of the correlated data, the recorded cross-power spectra were normalized by the corresponding auto-power spectra with the AIPS task ACCOR. Next, a priori amplitude calibration was applied with the task APCAL, which calculates the system equivalent flux density (SEFD) for each scan/station in the following way:

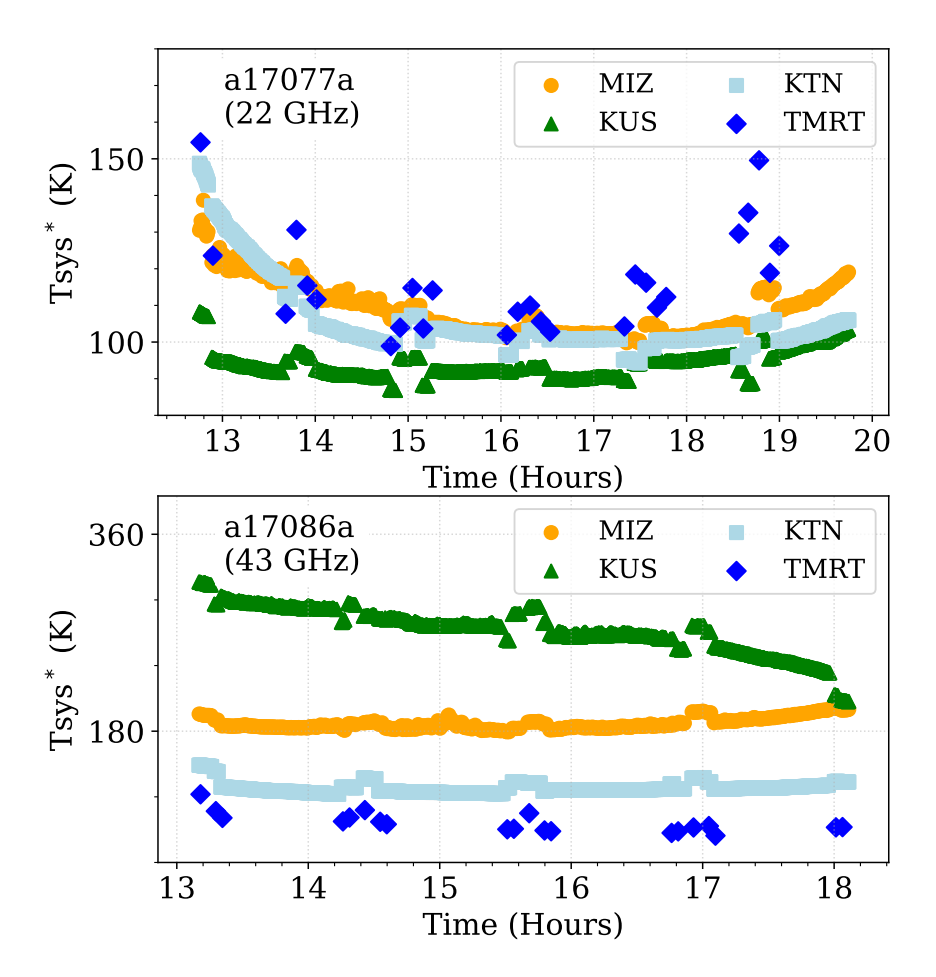


Figure 1: Opacity-corrected system temperature  $(T_{\rm sys}^{\star})$  of MIZ, KUS, KTN and TMRT in the a17077a (upper panel) and a17086a (lower panel).

$$SEFD = \frac{2k_{\rm B}T_{\rm sys}^{\star}}{A_{\rm e}} = \frac{8k_{\rm B}T_{\rm sys}e^{\tau}}{\eta_{\rm A}\pi D^2}(\rm Jy),\tag{1}$$

where  $k_{\rm B}$  is Boltzmann constant,  $T_{\rm sys}$  is the system noise temperature,  $\tau = \tau_0 \sec Z$  is the opacity at a zenith angle Z ( $\tau_0$  is the opacity at zenith), and  $A_{\rm e}$  is the antenna effective aperture area ( $A_{\rm e} = \pi \eta_{\rm A} D^2/4$ , where D is the antenna diameter and  $\eta_{\rm A}$  is the aperture efficiency). For KaVA data, the system temperature values stored in the log files are already opacity corrected (so-called  $T_{\rm sys}^{\star} = T_{\rm sys} \times e^{\tau}$ ), while those of TMRT are not corrected yet.

Hence, for TMRT we manually performed opacity corrections in AIPS/APCAL<sup>2</sup>. The fitting results of the zenith opacity and receiver temperature are ( $\tau_0 = 0.13$ ,  $T_{\rm rx} = 58\,\rm K$ ) for a17077a and ( $\tau_0 = 0.17$ ,  $T_{\rm rx} = 48\,\rm K$ ) for a17086a, which are consistent with the typical values measured at the site.

At the end of amplitude calibration, we further rescaled the whole visibility amplitude by a factor of 1.3 to properly correct the losses caused by multiple digitization processes in the KaVA/EAVN backend system and correlation (see [6] for more details). Note, however, that APCAL was not applied to NSRT due to the acquisition failure of  $T_{\rm sys}$  as described before. Instead, the amplitude of NSRT was recovered by making use of the point source imaging of 1219+044 (see section 2.3 for more details).

Following the apriori calibration, the amplitude was further corrected over frequencies. We performed bandpass calibration (task BPASS) for each antenna by using the auto-power spectra of 3C 273. We confirmed that the characteristic bandpass shape of each antenna was fully removed at this stage.

Obs. Code	$\nu^a$ (GHz)	Date	UT Time	Stations
a17077a	22	2017/03/18	12:45-19:45	KaVA (no KYS), TMRT, NSRT
a17086a	43	2017/03/27	13:10-18:10	KaVA, TMRT

Table 3: EAVN observations presented in this paper.  $^a$  Observing frequency. Observation target for both are M 87. The observation mode is  $32\,\mathrm{MHz} \times 8\,\mathrm{IFs}$ .

#### 2.2 Phase calibration

Following the amplitude calibration, we calibrated the visibility phases with the AIPS task FRING. First, using a scan of 3C 273 at a sufficient signal-to-noise ratio on each baseline  $(SNR_{ij} = S_{ij}/\sigma_{ij})$ , where  $S_{ij}$  is the received power and  $\sigma_{ij}$  is the noise level on a baseline i-j.), we derived and removed instrumental phase/delay offsets that are constant over the observing session. After the manual phase corrections, we performed a global fringe fitting over the whole scans and sources to fully remove phase/delay/rate residuals. Solution intervals of  $1 \,\mathrm{min}$  and  $30 \,\mathrm{s}$  (with  $SNR_{ij}$  threshold 5) were used for a 17077a and a 17086a, respectively, which are typical coherence time at each frequency. For both epochs, we successfully detected fringes on all baselines for most of the scans. In particular, when TMRT was used as the reference antenna, the fringe detection rate was significantly improved in both a17077a and a17086a thanks to its large collecting area. For comparison, in figure 2 we show  $SNR_{ij}$ obtained by FRING (on 3 baselines) for the point source 1219+044, for which the correlated flux densities are similar over the whole baselines. The measured SNR of KTN-TMRT at 22 GHz were  $\sim 4.4/\sim 3.4$  times higher than those of KTN-MIZ/KTN-KUS, which are consistent with our expectation under the bad weather condition. At 43 GHz, on the other hand, the measured SNR on KTN-TMRT was only  $\sim 4.2$  times higher than KTN-MIZ, which is  $\sim 30\%$  smaller than expected ( $\sim 6$  if we assume  $A_{\rm eff} = 45\%$  and calculate with practical

<sup>&</sup>lt;sup>2</sup>Note that the  $T_{\rm sys}$  measurements of TMRT were not as continuous as those of KaVA throughout EAVN sessions in 2017 (see figure 1). However, this issue has been fixed in 2018.

 $T_{\text{sys}}^{\star}$ ). The decrease of baseline SNR may be related to the reduction of aperture efficiency or/and pointing errors of TMRT, which will be discussed in section 3.

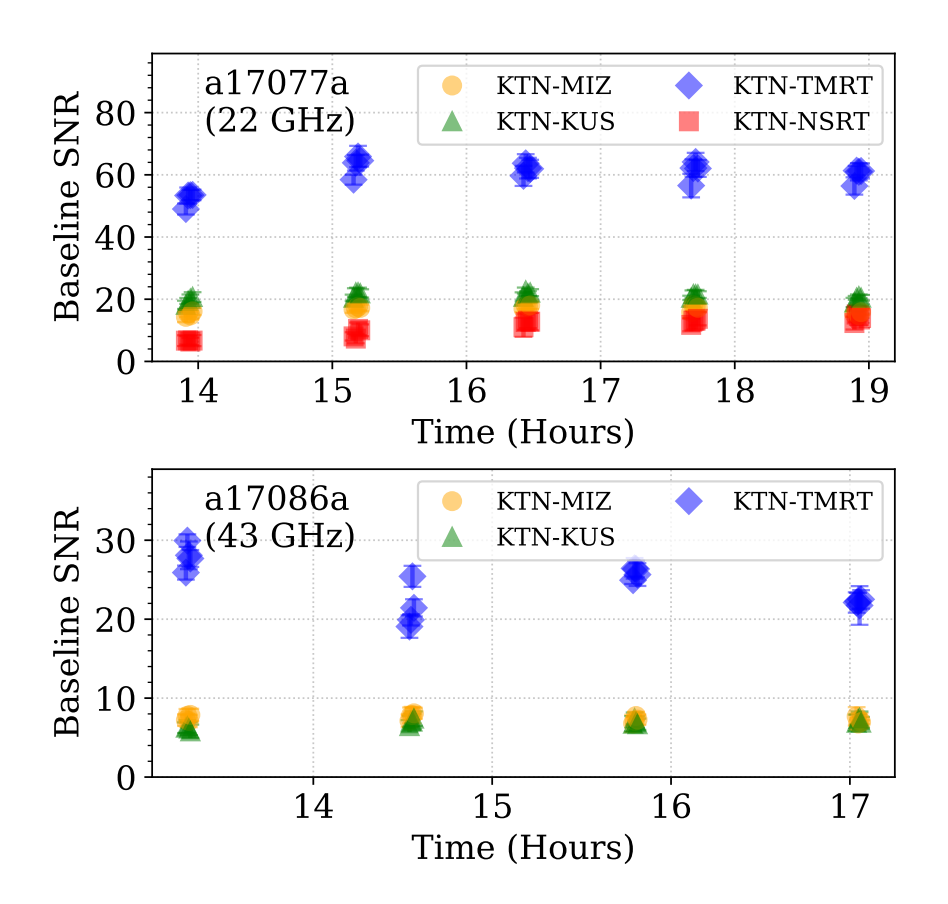


Figure 2: Baseline signal-to-noise ratio  $(SNR_{ij})$  (output from FRING) for various baselines for the point source 1219+044. (Upper panel) a17077a; (Lower panel) a17086a.

At 22 GHz, the SNR of KTN-NSRT is comparable with that of intra-KaVA baselines. This is broadly consistent with our expectation given the typical sensitivity of NSRT.

For M 84, the fringes at 43 GHz were not detected even with TMRT. This would be reasonable given the low core flux ( $\sim$ 100 mJy), relatively shorter integration time than a17077a, and the issues at TMRT described in section 3.

### 2.3 Imaging and self-calibration

The calibrated data were imported to DIFMAP for imaging and self-calibration. We conducted EAVN imaging in the following procedures. First, we flagged NSRT and TMRT because these stations contained large systematic offsets in the initial amplitude due to the absence of calibration (for NSRT) or due to large uncertainties in the applied information (for TMRT). Then, we first performed imaging/self-calibration for the point source 1219+044 only using KaVA, for which the apriori amplitude calibration is accurate within 10–15% [1, 5]. Since 1219+044 is known to be virtually unresolved on baseline lengths within

5078 km, the self-calibrated KaVA model of this source serves as an ideal amplitude reference for the remaining uncalibrated stations. We thus corrected the overall amplitude offsets of TMRT/NSRT by referencing to the source model obtained by KaVA. The amplitude correction factors of TMRT/NSRT derived from 1219+044 were also transferred to the scans of all the other sources. Then after removing the global amplitude offsets of TMRT/NSRT, we performed imaging/self-calibration with all the stations together to obtain final images for each source. All images were produced with a naturally-weighted scheme.

In figure 3 and 4, we show the visibility amplitude of 1219+044, 3C 273, M 84 and M 87 at 22/43 GHz as a function of uv-distance (note that M 84 was not detected at 43 GHz). In both figures, the left, middle and right panels are the visibility amplitude distributions with original apriori calibration, with the corrected apriori gain factors derived from the point-like source 1219+044, and with additional self-calibration, respectively. From the left and middle plots for 1219+044, one can clearly see that the amplitude offset between TMRT/NSRT and KaVA is almost removed by applying corrected gain factors. Since constant scaling factors were applied to all scans, there are small offsets caused by time variable gain components. However, the time variable residuals can be fully calibrated by self-calibration as shown in the right hand panels of figure 3/4

## 3 Amplitude offset of TMRT

The EAVN results presented here suggest an amplitude offset at 43 GHz by  $\sim 33\%$  between the baselines to TMRT and the ones among KaVA (see figure 4). Given that the corrections for digital signal processing and correlator [7] are properly implemented, the following possibilities are left to account for the remaining offset/loss of TMRT's amplitude: (a)  $T_{\rm sys}$  measurement, (b) opacity correction, (c) aperture efficiency, and (d) pointing accuracy.

For the two epochs presented here, the measured values of  $T_{\rm sys}$ ,  $T_{\rm rx}$  and atmospheric opacity at TMRT were all within the range of typical values. Therefore, we suspect that the latter two (c)(d) are the most likely causes. Below we briefly discuss the possible impact of each of these effects.

Aperture efficiency: For a parabolic antenna with an rms surface deviation error  $\epsilon$ , the aperture efficiency  $\eta_{\rm A}$  is known to be  $\eta_{\rm A}=e^{-(4\pi\epsilon/\lambda)^2}$  [8]. According to the TMRT observation log, the active surface controller did not properly work in a17086a. This suggests  $\epsilon$  for a17086a could be worse as large as  $\sim$ 0.6 mm [9]. At 22 GHz ( $\lambda=13\,\mathrm{mm}$ ), this level of deviation is still <1/20 of  $\lambda$  and should not seriously degrade the sensitivity/amplitude from what we expect. On the other hand, at 43 GHz ( $\lambda=7\,\mathrm{mm}$ ) the efficiency results in  $\eta_{\rm A}=0.31$ , which is significantly smaller than nominally adopted ( $\eta_{\rm A}=0.45$ ).

We can deduce the actual aperture efficiency of TMRT by comparing the observed fringe SNR on the point source 1219+044 between different baselines (see figure 2). If  $\eta_{A,TM} = 0.45$  as adopted in the a-priori calibration table, the SNR of KTN-TMRT should be 4.9 times higher than those of KTN-MIZ/KTN-KUS baselines, respectively. On the other hand, the actual improvement ratios were 3.4, which are 30% smaller than expected. If we assume that  $\eta_A$  of KTN, KUS and MIZ are all correct (as summarized in table 1), this directly reflects the TMRT efficiency loss, which is estimated to be  $\eta_{A,TM} \sim 70\% \times 45\% = 0.32$ . Indeed, this seems to be consistent with  $\eta_A$  for  $\epsilon = 0.6$  mm.

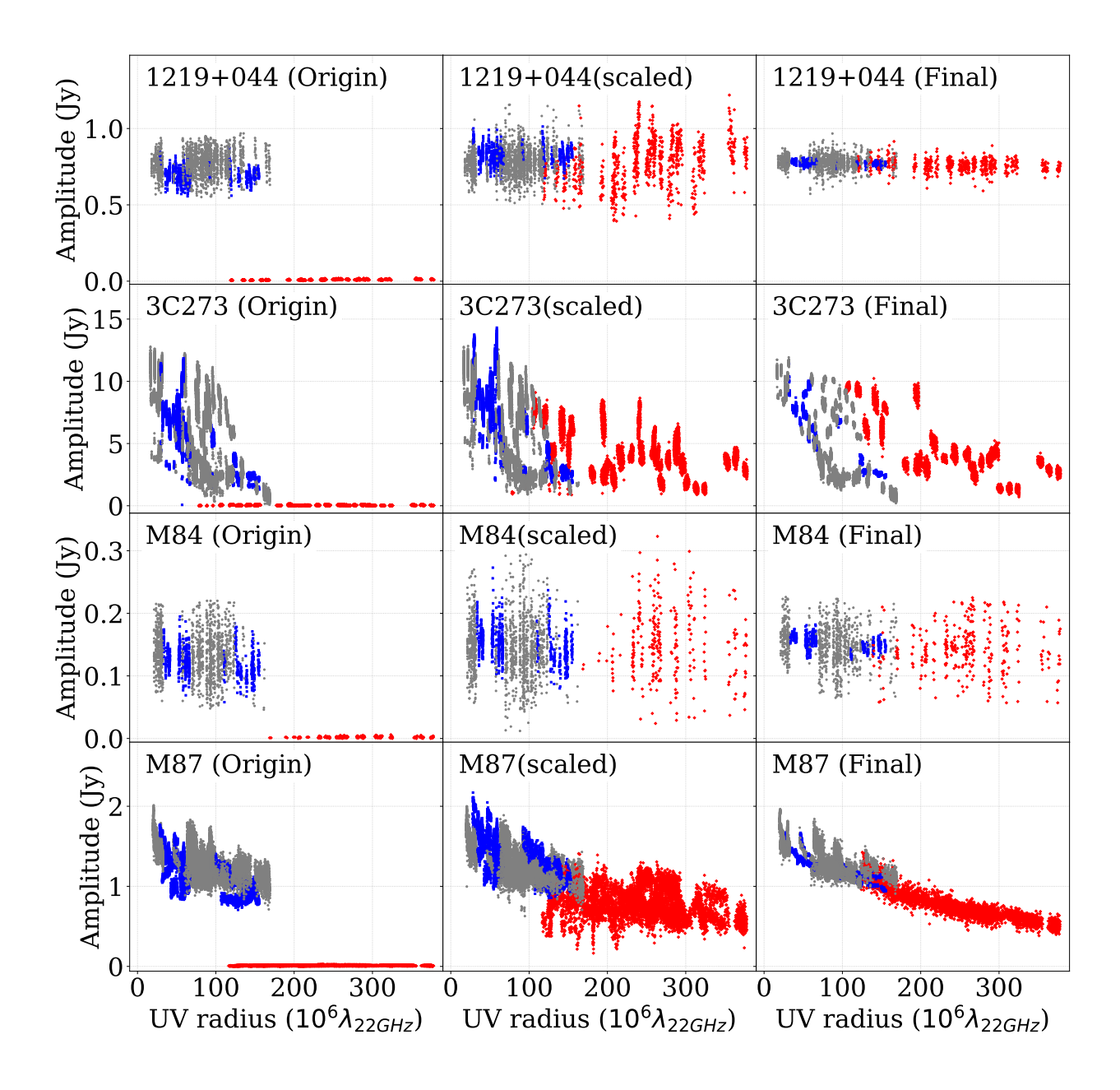


Figure 3: Visibility amplitude distributions as a function of uv-distance for a17077a. (Left) Data with original apriori calibration. (Middle) Data with corrected apriori gain values but before amplitude self-calibration. The scaling factor was obtained from the compact source 1219+044. (Right) Data after amplitude self-calibration. Red, blue and gray points indicate the data related to NSRT, TMRT and KaVA only, respectively. The visibility data are averaged every 2 mins.

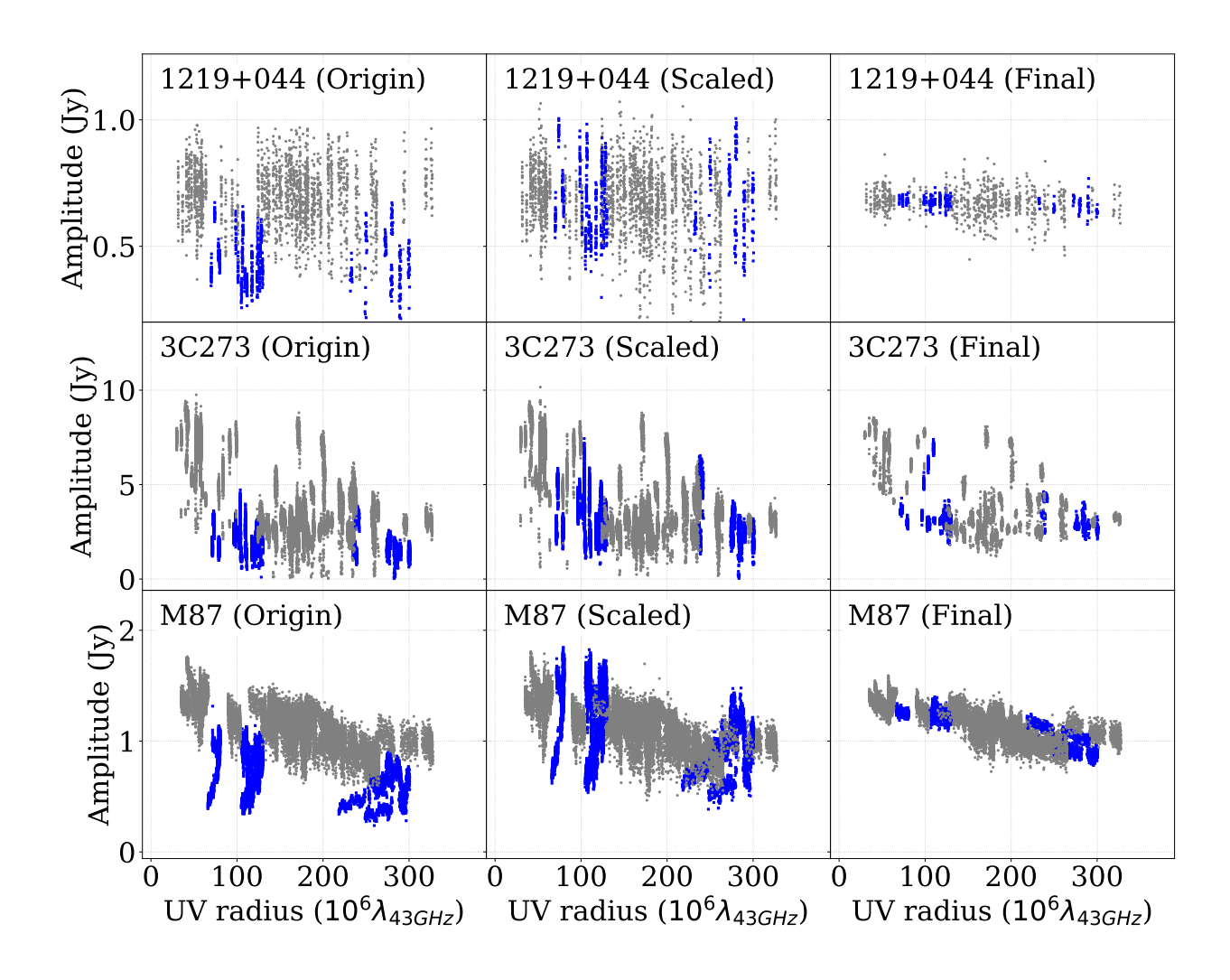


Figure 4: Same as figure 3 but for a17086a. The visibility data are averaged every 1 mins.

**Pointing accuracy:** This is an angular offset  $\sigma_{\theta}$  between the axes of the primary beam and the practical oriented direction, and the loss of receiving power is described by  $\Psi =$  $e^{-4\ln 2(\sigma_{\theta}/\Theta)^2}$  where  $\Theta$  is the HPBW of the main beam [?]. Pointing offsets are usually caused by the mechanical inaccuracy and deformation due to gravity and wind pressure, which are more sensitive for a large dish at high frequencies [?]. For TMRT, the typical pointing accuracy before and after pointing calibration is within  $\sim 10$  and  $\sim 3$  arcsecond, respectively, under modest ( $\sim 4 \,\mathrm{m\,s^{-1}}$ ) wind conditions. In the observations reported here (a17077a and a17086a), pointing calibration of TMRT was performed only prior to the sessions and no pointing slots were inserted during the sessions. Therefore the pointing accuracy of TMRT may gradually decrease with time. Here again let us focus on the KTN-TMRT 43 GHz SNR on 1219+044 shown in figure 2, where the highest SNR is seen on the first scan. If we assume that the observed SNR decrease on the later scans is fully caused by the increasing pointing offset of TMRT, we can estimate an additional/differential pointing offset  $\Delta \sigma_{\theta}$  for each scan with respect to the first scan, such that  $\Delta \sigma_{\theta} = 2\Theta \times \sqrt{\ln{(R_{\rm n1} - 0.5)}}$  (arcsecond), where  $R_{\rm n1} \equiv (SNR_{\rm scan-n}/SNR_{\rm scan-1})^2 = \Psi_{\rm TMRT, scan-n}/\Psi_{\rm TMRT, scan-1}$ . This results in  $\Delta\sigma_{\theta} =$ 8.67, 3.75, and 8.93 arcsecond for the 2nd/3rd/4th scans respectively, which implies a total uncertainty to be at most  $\sim 12$  arcsecond. Note that this level of pointing error is still sufficiently smaller than TMRT HPBW at 22 GHz (see table 1). This is consistent with the observed small ( $\sim 10\%$ ) differences in amplitude between KaVA and TMRT at 22 GHz.

Therefore, the observed amplitude offset of TMRT can be explained as the decreased aperture efficiency to  $\eta_{\rm A} \sim 31\%$  or the large pointing offset as  $\sim 12\,\rm arcsecond$ . In reality, both of the effects may contribute jointly, although the present data alone were difficult to conclude which of the two effects is more dominant. We note that, as of the writing of this article, the amplitude offset of TMRT seems to remain in more recent EAVN data conducted between 2017 and early 2020. Thus the investigation here provides a useful guide for the proper calibration of all the TMRT 43 GHz data obtained so far. To fix this issue, extensive work is ongoing at TMRT station. Once the amplitude offset is removed, the signal to noise ratio should increase. Therefore, the obtained array performance (sensitivity, imaging) based on these early commissioning data should be considered as a lower limit and a further improvement is expected once TMRT participates in the network with its full performance.

## References

- [1] Niinuma, K., Lee, S.-S., Kino, M., et al. 2014, PASJ, 66, 103
- [2] Hada, K., Park, J. H., Kino, M., et al. 2017, PASJ, 69, 71
- [3] Greisen, E. W. 2003, Information Handling in Astronomy Historical Vistas, 109
- [4] Shepherd, M. C., Pearson, T. J., & Taylor, G. B. 1994, BAAS, 26, 987
- [5] Cho, I., Jung, T., Zhao, G.-Y., et al. 2017, PASJ, 69, 87
- [6] Lee, S.-S., Byun, D.-Y., Oh, C. S., et al. 2015a, Journal of Korean Astronomical Society, 48, 229

- [7] Lee, S.-S., Oh, C. S., Roh, D.-G., et al. 2015b, Journal of Korean Astronomical Society, 48, 125
- [8] Ruze, J. 1966, IEEEP, 54, 633
- [9] Dong, J., Zhong, W., Wang, J., et al. 2018, IEEE Transactions on Antennas and Propagation, 66, 2044